Journal of Materials Chemistry A

ROYAL SOCIETY OF CHEMISTRY

PAPER

View Article Online
View Journal | View Issue

Cite this: J. Mater. Chem. A, 2025, 13, 5801

How thermally stable are vanadium cathode Li-ion cells?†

Fenghua Guo, [a] Hui Zhou, [a] Jonathan Miller,[a] Brian J. Schultz,[b] Leonardo Gobbato[bc] and M. Stanley Whittingham *[a]

Vanadium-based cathode materials are promising candidates for next-generation high energy batteries, as they are capable of enabling multi-electron redox reactions to host more than one Li^+ ion per vanadium atom. This work examined two vanadium cathodes (ζ-V_2O_5 and ε-$VOPO_4$) with respect to their electrochemical performance and thermal behaviors and compared the results with those of two commercial cathodes, $LiFePO_4$ (LFP) and $LiNi_{0.8}Mn_{0.1}Co_{0.1}O_2$ (NMC811). The two vanadium materials delivered much higher capacities (~300 mA h g^{-1} at *C*/20) than LFP and NMC811 as expected. They also presented comparable cycling and rate performance. Thermal evaluations on the charged samples in the presence of LP30 electrolyte by *ex situ* ARC and DSC measurements showed that they are significantly more stable than NMC811 and are comparable with LFP. Much larger heat generation was detected for both vanadium materials during normal charge and discharge through *in operando* thermal monitoring of the coin cells during cycling, which is ascribed to their complex reaction mechanism and huge polarization between charge and discharge. This did not harm their electrochemical performance and revealed that the increase in heat with cycling is similar to and even better than that of the NMC811 cathode.

Received 15th October 2024
Accepted 7th January 2025

DOI: 10.1039/d4ta07372j

rsc.li/materials-a

1 Introduction

The application of lithium-ion batteries (LIBs) has accelerated the development of portable electronic devices over the past few decades and is now rejuvenating the industry of electrical vehicles (EVs) after internal combustion engine powered vehicles took over the market in the first half of the 20th century.[1,2] High energy density is one of the core reasons behind the wide adoption of LIBs, and commercially available lithium-ion batteries on the market nowadays could reach around 250 W h kg^{-1}, a huge leap forward from 20–40 W h kg^{-1} a lead–acid battery can provide.[3–5] However, to push the full adoption of EVs, further increases in the energy density of LIBs are still desired.[1,3,6] Presently, commercialized cathode materials like lithium iron phosphate ($LiFePO_4$ or LFP) and nickel-rich layered oxides materials ($LiNi_xMn_yCo_{1-x-y}O_2$ or NMC, with $x \geq 0.6$) can only host one electron transfer per formula, which limits the available capacity. Materials that can facilitate multi-electron transfer are potential candidates to achieve much higher capacity and further enhance the energy density. Vanadium-based materials are intensively studied in this regard. As a transition metal, vanadium can form a variety of oxides and many of those were investigated for battery applications since the 1970s.[7–14] Layered vanadium pentoxide (α-V_2O_5) has been studied extensively over the past few decades and many different approaches have been tried to improve its slow kinetics.[7,11] A recent study showed that ζ-V_2O_5 has better cycling performance than α-V_2O_5, even though the initial capacity is a little lower.[15] ζ-V_2O_5 is a tunnel-structured vanadium oxide with building blocks of [VO_6] octahedra and [VO_5] square pyramids, where Li^+ could reside in multiple sites in the tunnel.[15,16] ζ-V_2O_5 resembles the structure of vanadium oxide bronzes β-$A_xV_2O_5$ (A = Na^+, Cu^{2+}, Ag^+, *etc.*) with the A ion removed.[16] It was reported that the tunnel structured ζ-V_2O_5 could deliver a discharge capacity of close to 250 mA h g^{-1} at *C*/4 in a voltage window of 2.0–4.0 V.[15] Besides vanadium oxides, other vanadium-based materials have also been extensively studied. For example, lithium vanadyl phosphate ($LiVOPO_4$) can accommodate more than one electron transfer.[17,18] Our group's previous work on ε-$VOPO_4$ showed that this olivine vanadyl phosphate was capable of reversibly de/lithiating two Li^+ ions and delivering a capacity of 305 mA h g^{-1}, which is 1.5 times the capacity of NMC and almost double the capacity of LFP.[19,20]

Although vanadium-based cathode materials have been investigated intensively over the past few decades and have been proven to provide much higher capacities, comprehensive studies on their thermal stability remain limited.[7,8,21] In this study, the thermal stabilities of two vanadium-based materials (ζ-V_2O_5 and ε-$VOPO_4$) at their charge states were investigated

[a]Department of Chemistry and Materials, State University of New York at Binghamton, Binghamton, New York 13902-6000, USA. E-mail: stanwhit@gmail.com
[b]Dimien Inc., Buffalo, New York 14228, USA
[c]Department of Chemical and Biological Engineering, State University of New York at Buffalo, Buffalo, New York 14260-4200, USA

† Electronic supplementary information (ESI) available. See DOI: https://doi.org/10.1039/d4ta07372j

and their thermal behaviors during normal electrochemical operation were evaluated with an *operando* calorimeter. As a comparison, two commercialized cathode materials (LFP and NMC811) were also tested under the same conditions. It was found that the thermal stabilities of the two vanadium-based materials (ζ-V_2O_5 and ε-$VOPO_4$) are comparable with that of LFP and are better than that of NMC811 in a thermal runaway event.

2 Methodology

2.1 Materials synthesis

LFP was purchased from MTI Corp. ($LiFePO_4$, Model#: EQ-Lib-LFPO-S21) and NMC811 was purchased from Targray (NMC811 80% Ni, LOT#: LT-180180070). ζ-V_2O_5 was received from Dimien Inc., where it was synthesized through a hydrothermal method starting with the synthesis of β-$Ag_{0.33}V_2O_5$, followed by leaching out Ag^+ ions from the tunnel. The detailed method can be found in a previous publication by Luo.[15] The obtained ζ-V_2O_5 was vacuum dried at 120 °C overnight before use. ε-$VOPO_4$ was synthesized by first obtaining H_2VOPO_4 through hydrothermal synthesis, followed by annealing under an oxygen flow. The full synthesis method can be found in our group's previous publication by Siu.[19]

2.2 Materials characterization

X-ray diffraction (XRD) patterns were collected with a Bruker diffractometer (D8 Advance, Cu Kα source, $\lambda = 1.5418$ Å). SEM images were collected with a field emission SEM (Zeiss SUPRA 55 VP) at 15 kV operating voltage.

2.3 Electrochemical measurements

For electrochemical measurements with coin cells, the electrodes were prepared by mixing the active material, graphene (NanoPlatelets, xGnP C-750, XG Sciences) and poly(vinylidene fluoride) (PVDF) with a weight ratio of 80 : 10 : 10. To ensure good contact between the active material and graphene, they were first manually mixed for ~40 min using a mortar and pestle. The mixture was then collected and added with PVDF and *N*-Methylpyrrolidone (NMP) to form a slurry using a mixer (Thinky ARE 310). The slurry was then cast onto carbon-coated Al foil using a doctor blade. After drying, the coated electrode sheet was punched into electrode discs with a diameter of 12.7 mm and then calendared to 2.0 g cm^{-3} of active material. The calendared electrodes were vacuum dried at 120 °C for 2 h and then transferred to an argon-filled glove box for cell assembly. The average mass loading of the obtained electrodes was 9.8 mg of active material, with a variation between 8.4 and 13.0 mg. The coin cell (2032-type, cell parts from Hohsen, Japan) was assembled with a lithium chip (600 μm in thickness) as the anode, 50 μL of LP30 (1 M lithium hexafluorophosphate ($LiFP_6$) in ethylene carbonate (EC) and dimethyl carbonate (DMC) with a volume ratio of 50/50) as the electrolyte, and one layer of polyethylene separator (Energy Tech Solution Co.).

The electrochemical measurements started with two formation cycles at *C*/10. The current density and voltage window varied per cathode material, as shown in Table S1.† For cycling performance measurements, the current density was *C*/5 for charge and *C*/3 for discharge. Cycle numbers in this paper are counted without formation cycles. The electrochemistry measurements were conducted with BioLogic cyclers.

2.4 Thermal measurements

Charged powders for thermal measurements were prepared differently. The powders for Thermogravimetric Analysis with Mass Spectrometry (TGA-MS) measurements were scratched off from coin cell electrodes. The powders for Accelerating Rate Calorimetry (ARC) and Differential Scanning Calorimetry (DSC) measurements were prepared as pouch cells. The pouch cell electrodes were prepared the same way as coin cell electrodes without punching or calendaring, except that Al foil without carbon coating was used for LFP due to difficulties in recovering the charged powders. The average size of the cathode in a pouch cell was 8 × 7.7 cm (average loading: 0.49 g), paired with a lithium metal anode (50 μm in thickness, plated on copper foil, 8.5 × 10 cm in size). The amount of electrolyte used for each cell was roughly 4 times the mass of active materials. The pouch cell used for the ARC trial run was prepared differently, and the procedure would be described along with the data shown in the ESI.† All the charged powders were collected after two formation cycles followed by one charge segment to its upper potential window at *C*/10 and a 24 h rest. The electrodes were washed with dimethyl carbonate and dried under vacuum for 20 min before the powders were collected.

2.4.1 *Operando* calorimetry. *Operando* calorimetry was conducted using a TAM IV calorimeter (TA Instruments) with a coin cell lifter. The measurements were done with coin cells under isothermal conditions for two formation cycles and the first 3 cycles of every 20 cycles, with temperature holding at 30 °C. The rest of the cycles were performed at room temperature outside of the calorimeter. Between each charge or discharge segment, there was a 6 h rest period to collect in-measurement baselines. When calculating the cycle heat, the integration was done from the start of charge to 1 h after discharge since heat transfer lags behind after discharge finished. Heat flow was normalized by the mass of the cathode active material.

2.4.2 Accelerating rate calorimetry. ARC measurements were conducted using the MMC 274 with the ARC module (NETZSCH). The 'Heat-Wait-Search' method was used from 100 °C to 350 °C with a temperature increment of 10 °C. The waiting period was 30 min, followed by 10 min of 'Search'. The threshold for self-heating was set to 0.05 K min^{-1}. Approximately 270 mg charged active material (corresponding to 337.5 mg electrode powder) with ~135 mg LP30 was loaded into a stainless-steel vessel (volume inside: 2.6 mL) inside an Argon-filled glovebox and the opening was covered with parafilm before transferring it out. The ratio between the cathode active material and electrolyte was 2 : 1, similar to the ratio used in MacNeil's work.[22] When loading the vessel into the instrument, there was exposure to air for a few seconds . The total volume of the vessel (excluding the volume of tubes connected to the vent and pressure sensor) was 2.6 mL, which is insignificant

compared to 328 mL of air needed for the total combustion of solvents from 135 mg LP30, calculated from the ideal gas law.

2.4.3 Differential scanning calorimetry. DSC measurements were carried out with a Discovery DSC 250 (TA Instruments), using an aluminium-coated stainless steel high pressure pan with a gold-plated copper inner cover. Around 5 mg charged cathode active material (corresponding to 6.25 mg electrode powder) with ~2.5 mg LP30 (the same powder to electrolyte ratio as in the ARC measurements) was added to the sample capsule. The measurements were performed from 50 °C to 300 °C with a heating rate of 2.5 °C min^{-1}, under a constant N_2 flow at 50 mL min^{-1} as a protecting gas. Heat flow was normalized by the total mass of electrode powder and electrolyte. Heat generation was calculated by integrating from 100 °C to 300 °C using the value at 100 °C as the baseline.

2.4.4 Thermogravimetric analysis with mass spectrometry. TGA-MS measurements were done with a Netzsch TG 209 F1 Iris with a QMS 403 Aëolos. The average loading of charged powder was 8.4 mg. Samples were heated in an Al_2O_3 crucible from room temperature to 400 °C at a heating rate of 10 °C min^{-1} under argon flow.

3 Results and discussion

The particle morphologies and X-ray diffraction patterns of the 4 cathode materials are shown in Fig. S1.† The various materials have different morphologies: ζ-V_2O_5 is composed of nano-rods with lengths on the order of several microns, while the width is in the sub-micron range; ε-$VOPO_4$ and LFP have sub-micron sized primary particles that tend to form loose clusters; NMC811 is composed of typical micron-sized "meatball" shaped secondary particles close-packed with sub-micron primary particles. The XRD study verified the pure phase for each material.

The electrochemical evaluations for these four different cathode materials are compared in Fig. 1. Similar to earlier reports,[15,19] benefited from the two-electron redox reaction between $V^{5+} \leftrightarrow V^{4+} \leftrightarrow V^{3+}$, the two vanadium-based cathodes gave capacities close to 300 mA h g^{-1} at lower current rates (Fig. 1(a)), which is much higher than the two commercialized cathodes, LFP and NMC811, with only a single-electron reaction. For the cycling performance at *C*/5 charge and *C*/3 discharge, although LFP presented the best cyclability with no capacity lost after 100 cycles (increased by 1.3%), the two vanadium-based cathodes showed comparable performance with the NMC811 cathode (capacity retention was 87.4%, 89.8%, and 93.0% for NMC811, ζ-V_2O_5 and ε-$VOPO_4$, respectively) and still had a capacity of above 220 mA h g^{-1} after 100 cycles (Fig. 1(b)).

From the rate performance shown in Fig. 1(c and d), ζ-V_2O_5 exhibited the best rate capability among the four materials, with 91.0% discharge capacity retention when the current density increased from *C*/20 to 1C, which may be ascribed to its higher conductivity and nano-rod morphology. The capacity retention for LFP and NMC811 fell behind that of ζ-V_2O_5, at 85.7% and 76.9%, respectively. Although ε-$VOPO_4$ only retained 67.0% of its initial discharge capacity when the current density was increased from *C*/20 to 1C, the discharge capacity at 1C was still able to reach ~200 mA h g^{-1}, higher than that of LFP and NMC811 (Fig. 1(c)).

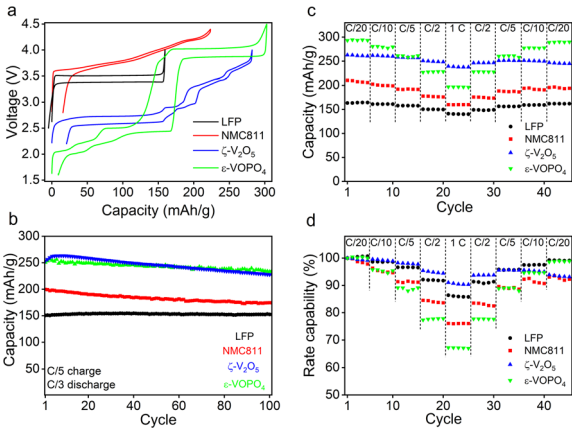

Fig. 1 Electrochemical performance of the four different cathode materials, ζ-V_2O_5, ε-$VOPO_4$, LFP and NMC811, in coin cells: (a) voltage profile at *C*/20 for charge/discharge; (b) cyclability over 100 cycles at *C*/5 charge and *C*/3 discharge; rate performance from *C*/20 to 1C, plotted in (c) absolute value and (d) percentage.

3.1 Thermal stability evaluated with *ex situ* calorimetry and mass spectrometry

The above electrochemical comparison clearly manifested the apparent advantages of the two vanadium-based cathode materials (ζ-V_2O_5 and ε-$VOPO_4$) over the two commercial cathodes (LFP and NMC811). How about their thermal stabilities? One of the concerns regarding nickel-rich materials is the thermally unstable [$Ni^{4+}O_6$] octahedra, which may release oxygen and trigger a thermal runaway event.[23–25] We addressed whether vanadium-based materials face such issues.

The thermal stability of ζ-V_2O_5 and ε-$VOPO_4$ at their charged states and their reactivity with LP30 electrolyte were evaluated by *ex situ* ARC and DSC measurements, and the results are shown in Fig. 2 and S2–S4.† As shown in Fig. 2, ζ-V_2O_5 and ε-$VOPO_4$ electrodes experienced similar temperature changes with LFP during the "heat-wait-search" process in ARC measurements starting from 100 °C, where periodic unsustained self-heating periods existed between 150 °C and 350 °C, indicating that some exothermic reactions occurred. Those exothermic reactions proceeded with very small self-heating rates (<0.2 K min^{-1}) (Fig. S4†), which are well below 10 K min^{-1}, the onset of thermal runaway,[26] indicating just minor heat release at those temperatures. These should not be harmful to the safety of the battery. In contrast, NMC811 exhibited a distinct temperature profile where self-heating started around 175 °C, and a dramatic increase happened from ~188 °C, resulting in a large self-heating rate far above the onset of thermal runaway (Fig. S4†), revealing the poor thermal stability of the NMC811 cathode material.

The XRD patterns of the ARC products (Fig. S5 and Table S2†) showed that all four charged samples experienced

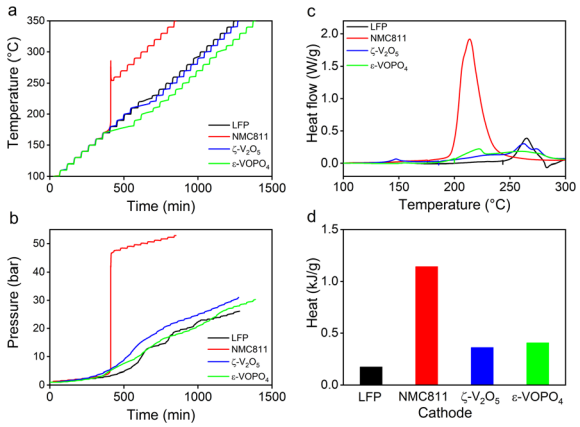

Fig. 2 Thermal stability of the four different cathode materials, ζ-V_2O_5, ε-$VOPO_4$, LFP and NMC811, at charged states in the presence of LP30 measured by ARC: (a) temperature profiles and (b) pressure during the "heat-wait-search" mode, as well as DSC: (c) heat flow profile and (d) integrated heat.

reduction reactions during ARC, by losing oxygen from their structure. This may explain the observed pressure increases during the ARC measurements (Fig. 2(b)). The pressure change profiles matched very well with the temperature changing profiles: ζ-V_2O_5, ε-$VOPO_4$ and LFP charged samples showed gradual pressure increases with time except for some small jumps in the pressure corresponding to the minor exothermic reactions detected in Fig. 2(a). The NMC811 charged sample still gave a distinct pressure change profile from the other three, which had a dramatic rise at 180 °C, the onset temperature for thermal runaway. This dramatic pressure rise indicates that a substantial amount of gas was produced at that moment, especially oxygen, which created an "explosive" environment that contributed to the further reduction of NiO to Ni metal, as evidenced by the strong diffraction peaks from Ni shown in Fig. S5(b).† The TGA-MS data collected on charged samples in the absence of LP30 (Fig. S6†) verified our speculation about the oxygen release: a significant O_2 release peak was detected for charged NMC811 starting around 200 °C, indicating the very poor thermal stability of the charged NMC811 cathode, which can easily lose the oxygen from its structure.

ζ-V_2O_5, ε-$VOPO_4$ and LFP at their charged states were known to be stable by themselves below 400 °C.[15,21,27] However, in the presence of electrolyte, charged LFP decomposes and loses oxygen at a very slow speed and forms $Fe_2P_2O_7$.[28] Our team's previous thermal studies on the ε-$VOPO_4$ cathode also found that the existence of electrolyte could worsen its thermal stability.[21] Based on the species identified using XRD data from the ARC products shown in Fig. S5,† this is likely also the case for ζ-V_2O_5, and some of the possible decomposition reactions for ζ-V_2O_5, ε-$VOPO_4$ and LFP could be described in eqn (1)–(4).

$$V_2O_5 \rightarrow 2VO_2 + 1/2O_2 \quad (1)$$

$$VO_2 \rightarrow VO + 1/2O_2 \quad (2)$$

$$VOPO_4 \rightarrow VPO_4 + 1/2O_2 \quad (3)$$

$$2FePO_4 \rightarrow Fe_2P_2O_7 + 1/2O_2 \quad (4)$$

The slow release of oxygen eventually caused periodic exothermic reactions but not to a degree sufficient to trigger thermal runaway.

DSC measurements on the four charged cathodes in the presence of LP30 electrolyte (Fig. 2(c and d)) strongly support the ARC data. Charged NMC811 generated the largest heat release of 1142 J g^{-1} and the lowest onset temperature, while charged ζ-V_2O_5 and ε-$VOPO_4$ released only less than half of that heat, 361 J g^{-1} and 406 J g^{-1}, respectively. Charged LFP showed the least heat generation among the four materials, with just 173 J g^{-1} of heat released under the same conditions. Furthermore, the intensity of maximum heat flux for NMC811 is more than four times that of ζ-V_2O_5 or ε-$VOPO_4$, as shown in Table S3.†

So, based on the ARC and TGA-MS results, as well as DSC data, the thermal stability of the two vanadium-based materials (ζ-V_2O_5 and ε-$VOPO_4$) is comparable with that of LFP and much better than that of NMC811, in the order of LFP > ζ-V_2O_5 ≈ ε-$VOPO_4$ ≫ NMC811.

3.2 *In operando* monitoring of heat generation during cycling

Ex situ studies confirmed the comparable thermal stabilities of the two vanadium-based cathode materials (ζ-V_2O_5 and ε-$VOPO_4$) to commercial cathode material LFP, but much better than that of the commercial cathode materials NMC811 during a dynamic heating process. Considering real applications, it is also important to evaluate their thermal behaviors under normal operational conditions.

As shown in Fig. 3 and S7,† heat generation was monitored *in operando* for coin cells made with the four different cathodes (ζ-V_2O_5, ε-$VOPO_4$, LFP and NMC811) through a Thermal Analysis Microcalorimeter (TAM IV) during their cycling at *C*/5 for charge and *C*/3 for discharge. All four cells showed significant heat generation at the end of discharge, where voltage changes dramatically with lithiation. Similar phenomena were observed for the intense peak for ε-$VOPO_4$ in the transition region between the two plateaus around 2.5 V and 4.0 V. This type of heat generation could be attributed to the rapid increase in overpotential and slower lithium diffusion, causing spikes in heat generation.[29]

ζ-V_2O_5 has multiple charge/discharge plateaus, which resulted from Li^+ re-ordering in the tunnel structure at different voltages.[15] Accordingly, the heat generation profile showed multiple heat flux spikes corresponding to the voltage transition region between the plateaus. These spikes could again be attributed to the sudden increase in overpotential.

Comparatively, the heat signals are smooth for NMC811 and LFP, due to their simple reaction mechanism. There was a solid-solution reaction for NMC811 between 2.8 V and 4.4 V and no dramatic change occurred to the layer structure.[30] The slightly higher heat generation at the beginning of charge around 3.6 V

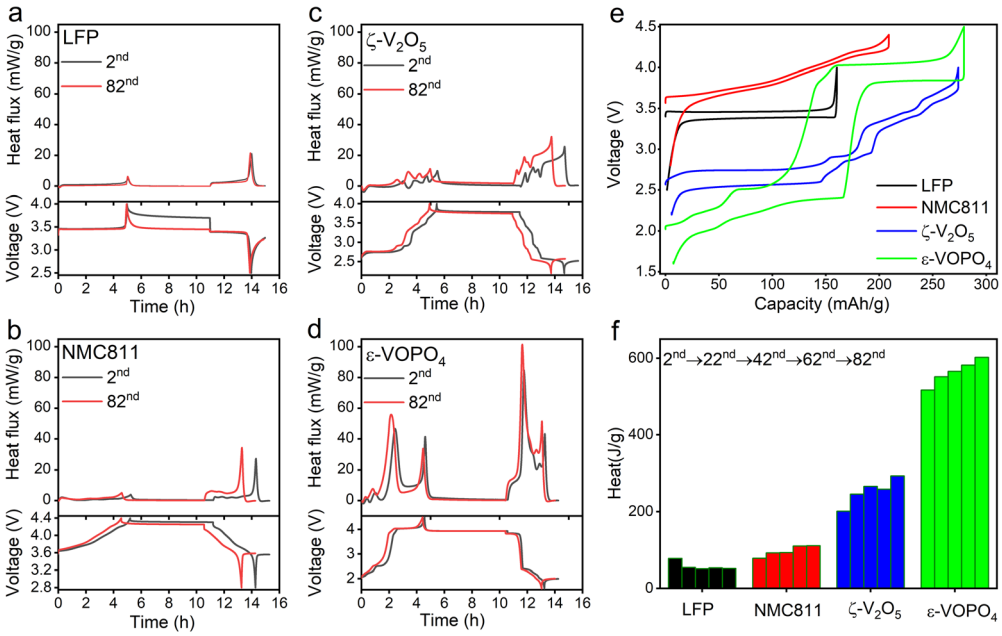

Fig. 3 (a–d) Heat flux and charge/discharge profile of 2nd cycle and 82nd cycle for the four cells, (e) comparison of charge/discharge profiles of 2nd cycle, and (f) calculated heat generation over one full cycle in different cycles. The cells were measured at *C*/5 for charge and *C*/3 for discharge.

was likely due to sluggish Li^+ diffusion and high charge transfer resistance.[30,31] For LFP, a long stable plateau around 3.5 V resulted from a two-phase reaction mechanism, which dominated the entire electrochemical process.[32]

The heat generation during one full cycle (2nd cycle) was integrated and compared in Fig. 3(f) as well as their changes over cycling. ε-$VOPO_4$ showed the most intensive heat flux (Fig. 3(d)) and gave the largest heat generation (516.76 J g^{-1}) among the four cells. The poor electronic conductivity of ε-(Li)$VOPO_4$ is likely one of the reasons.[18] The largest polarization between the charge and discharge curves for ε-$VOPO_4$ (Fig. 3(e)), which caused the lowest energy efficiency (Fig. S8†), could be another cause. ζ-V_2O_5 generated 201.12 J g^{-1} of heat, which is much lower than that of ε-$VOPO_4$ but still much higher than the heat generated by LFP or NMC811, which was only 77.63 J g^{-1} and 78.16 J g^{-1}, respectively. This could be attributed to its complex reaction mechanism. Although the two vanadium-based cathodes generated significant heat during one cycle operation, the growth of heat generation with cycling is similar to or even better than that of the NMC811 cathode: the growth ratio of heat generation from 2nd cycle to 82nd cycle for ζ-V_2O_5 is 46%, a similar ratio to that of NMC811 at 42%. ε-$VOPO_4$ was even lower at 17%. LFP is still the best among the four materials, with almost no change after the 2nd cycle, showing very high stability.

4 Conclusions

The electrochemical and thermal properties of two vanadium-based cathode materials (ζ-V_2O_5 and ε-$VOPO_4$) were investigated and compared with those of commercial LFP and NMC811 cathodes. Both ζ-V_2O_5 and ε-$VOPO_4$ showed much higher capacity (close to 300 mA h g^{-1}) due to their ability to accommodate more than one Li^+ ion per vanadium atom. Their thermal stabilities at elevated temperatures are comparable with that of LFP but significantly higher than that of NMC811 due to their stable structures. ζ-V_2O_5 and ε-$VOPO_4$ generate much more heat during the normal charge and discharge operation, which reduces their energy efficiency. Their cycling stability, however, is not affected by high cycle heat. Overall, ζ-V_2O_5 and ε-$VOPO_4$ are both promising candidates for thermally stable and high-capacity cathode materials.

Data availability

All data supporting the results of this article are included in the article and/or the ESI.†

Author contributions

Fenghua Guo: investigation, methodology, data curation, formal analysis, validation, and writing – original draft; Hui Zhou: conceptualization, investigation, methodology, and writing – editing; Jonathan Miller: resources, editing; Brian J. Schultz: funding acquisition, conceptualization, and project administration; Leonardo Gobbato: resources; M. Stanley Whittingham: funding acquisition, conceptualization, writing – editing, project administration, and supervision. All the authors participated in reviewing the manuscript.

Conflicts of interest

There are no conflicts to declare.

Acknowledgements

This work was supported by the U.S. National Science Foundation Small Business Technology Transfer Award under award number 2112152. The authors thank TA Instruments for providing the coin-cell lifters for the TAM IV used for *operando* calorimetry, and for their continued assistance.

References

1 M. Li, J. Lu, Z. Chen and K. Amine, *Adv. Mater.*, 2018, **30**, 1800561.
2 A. Ajanovic, *Wiley Interdiscip. Rev.:Energy Environ.*, 2015, **4**, 521–536.
3 M. S. Whittingham and J. Xiao, *MRS Bull.*, 2023, **48**, 1118–1124.
4 M. M. Thackeray, C. Wolverton and E. D. Isaacs, *Energy Environ. Sci.*, 2012, **5**, 7854–7863.
5 J. M. Tarascon and M. Armand, *Nature*, 2001, **414**, 359–367.
6 J. B. Goodenough and K.-S. Park, *J. Am. Chem. Soc.*, 2013, **135**, 1167–1176.
7 X. Zhang, X. Sun, X. Li, X. Hu, S. Cai and C. Zheng, *J. Energy Chem.*, 2021, **59**, 343–363.
8 X. Xu, F. Xiong, J. Meng, X. Wang, C. Niu, Q. An and L. Mai, *Adv. Funct. Mater.*, 2020, **30**, 1904398.
9 J. Yao, Y. Li, R. C. Massé, E. Uchaker and G. Cao, *Energy Storage Mater.*, 2018, **11**, 205–259.
10 M. S. Whittingham, Y. Song, S. Lutta, P. Y. Zavalij and N. A. Chernova, *J. Mater. Chem.*, 2005, **15**, 3362–3379.
11 M. S. Whittingham, *Chem. Rev.*, 2004, **104**, 4271–4302.
12 K. West, B. Zachau-Christiansen, M. J. L. Østergård and T. Jacobsen, *J. Power Sources*, 1987, **20**, 165–172.
13 D. W. Murphy, P. A. Christian, F. J. DiSalvo and J. N. Carides, *J. Electrochem. Soc.*, 1979, **126**, 497.
14 D. W. Murphy and P. A. Christian, *Science*, 1979, **205**, 651–656.
15 Y. Luo, S. Rezaei, D. A. Santos, Y. Zhang, J. V. Handy, L. Carrillo, B. J. Schultz, L. Gobbato, M. Pupucevski, K. Wiaderek, H. Charalambous, A. Yakovenko, M. Pharr, B.-X. Xu and S. Banerjee, *Proc. Natl. Acad. Sci. U. S. A.*, 2022, **119**, e2115072119.
16 P. M. Marley, T. A. Abtew, K. E. Farley, G. A. Horrocks, R. V. Dennis, P. Zhang and S. Banerjee, *Chem. Sci.*, 2015, **6**, 1712–1718.
17 L. W. Wangoh, S. Sallis, K. M. Wiaderek, Y.-C. Lin, B. Wen, N. F. Quackenbush, N. A. Chernova, J. Guo, L. Ma, T. Wu, T.-L. Lee, C. Schlueter, S. P. Ong, K. W. Chapman, M. S. Whittingham and L. F. J. Piper, *Appl. Phys. Lett.*, 2016, **109**, 053904.
18 Y.-C. Lin, B. Wen, K. M. Wiaderek, S. Sallis, H. Liu, S. H. Lapidus, O. J. Borkiewicz, N. F. Quackenbush, N. A. Chernova, K. Karki, F. Omenya, P. J. Chupas, L. F. J. Piper, M. S. Whittingham, K. W. Chapman and S. P. Ong, *Chem. Mater.*, 2016, **28**, 1794–1805.
19 C. Siu, I. D. Seymour, S. Britto, H. Zhang, J. Rana, J. Feng, F. O. Omenya, H. Zhou, N. A. Chernova, G. Zhou, C. P. Grey, L. F. J. Piper and M. S. Whittingham, *Chem. Commun.*, 2018, **54**, 7802–7805.
20 L.-X. Yuan, Z.-H. Wang, W.-X. Zhang, X.-L. Hu, J.-T. Chen, Y.-H. Huang and J. B. Goodenough, *Energy Environ. Sci.*, 2011, **4**, 269–284.
21 Y. Huang, Y. C. Lin, D. M. Jenkins, N. A. Chernova, Y. Chung, B. Radhakrishnan, I. H. Chu, J. Fang, Q. Wang, F. Omenya, S. P. Ong and M. S. Whittingham, *ACS Appl. Mater. Interfaces*, 2016, **8**, 7013–7021.
22 D. D. MacNeil and J. R. Dahn, *J. Electrochem. Soc.*, 2001, **148**, A1205.
23 W. M. Dose, I. Temprano, J. P. Allen, E. Björklund, C. A. O'Keefe, W. Li, B. L. Mehdi, R. S. Weatherup, M. F. L. De Volder and C. P. Grey, *ACS Appl. Mater. Interfaces*, 2022, **14**, 13206–13222.
24 W. Liu, P. Oh, X. Liu, M.-J. Lee, W. Cho, S. Chae, Y. Kim and J. Cho, *Angew. Chem., Int. Ed.*, 2015, **54**, 4440–4457.
25 H.-J. Noh, S. Youn, C. S. Yoon and Y.-K. Sun, *J. Power Sources*, 2013, **233**, 121–130.
26 K. Liu, Y. Liu, D. Lin, A. Pei and Y. Cui, *Sci. Adv.*, 2018, **4**, eaas9820.
27 J. Kim, K.-Y. Park, I. Park, J.-K. Yoo, J. Hong and K. Kang, *J. Mater. Chem.*, 2012, **22**, 11964–11970.
28 P. Röder, N. Baba, K. A. Friedrich and H. D. Wiemhöfer, *J. Power Sources*, 2013, **236**, 151–157.
29 R. Essehli, R. Amin, A. Abouimrane, M. Li, H. ben Yahia, K. Maher, Y. Zakaria and I. Belharouak, *ChemSusChem*, 2020, **13**, 5031–5040.
30 K. Märker, P. J. Reeves, C. Xu, K. J. Griffith and C. P. Grey, *Chem. Mater.*, 2019, **31**, 2545–2554.
31 I. McClelland, S. G. Booth, N. N. Anthonisamy, L. A. Middlemiss, G. E. Pérez, E. J. Cussen, P. J. Baker and S. A. Cussen, *Chem. Mater.*, 2023, **35**, 4149–4158.
32 A. K. Padhi, K. S. Nanjundaswamy and J. B. Goodenough, *J. Electrochem. Soc.*, 1997, **144**, 1188.

